



저작자표시-비영리-변경금지 2.0 대한민국

이용자는 아래의 조건을 따르는 경우에 한하여 자유롭게

- 이 저작물을 복제, 배포, 전송, 전시, 공연 및 방송할 수 있습니다.

다음과 같은 조건을 따라야 합니다:



저작자표시. 귀하는 원저작자를 표시하여야 합니다.



비영리. 귀하는 이 저작물을 영리 목적으로 이용할 수 없습니다.



변경금지. 귀하는 이 저작물을 개작, 변형 또는 가공할 수 없습니다.

- 귀하는, 이 저작물의 재이용이나 배포의 경우, 이 저작물에 적용된 이용허락조건을 명확하게 나타내어야 합니다.
- 저작권자로부터 별도의 허가를 받으면 이러한 조건들은 적용되지 않습니다.

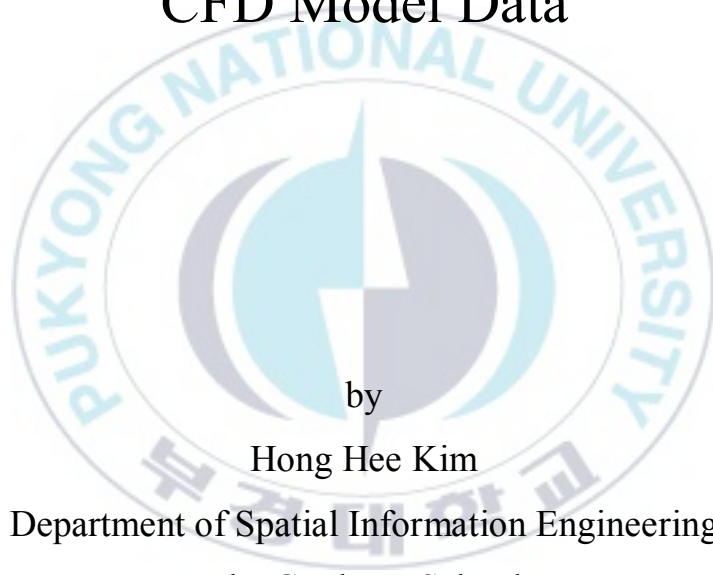
저작권법에 따른 이용자의 권리는 위의 내용에 의하여 영향을 받지 않습니다.

이것은 [이용허락규약\(Legal Code\)](#)을 이해하기 쉽게 요약한 것입니다.

[Disclaimer](#)

Thesis for the Degree of Master of Engineering

# Retrieval of High Resolution Surface Net Radiation for Urban Area Using Satellite Remote Sensing Technique and CFD Model Data



by

Hong Hee Kim

Department of Spatial Information Engineering

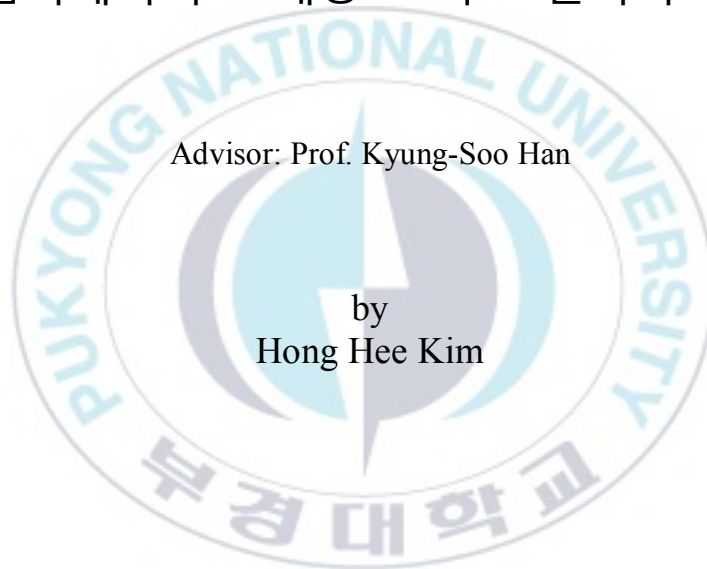
The Graduate School

Pukyong National University

February 2018

# Retrieval of High Resolution Surface Net Radiation for Urban Area Using Satellite Remote Sensing Technique and CFD Model Data

(위성 원격탐사 기법과 CFD 모델 자료를 활용한  
도심지에서의 고해상도 지표 순복사 산출)



Advisor: Prof. Kyung-Soo Han

by  
Hong Hee Kim

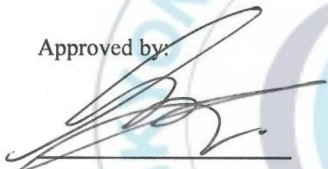
A thesis submitted in partial fulfillment of the requirements  
for the degree of  
Master of Engineering  
in Department of Spatial Information Engineering, The Graduate School,  
Pukyong National University

February 2018

Retrieval of High Resolution Surface Net Radiation for Urban  
Area Using Satellite Remote Sensing Technique and  
CFD Model Data

A dissertation  
by  
Hong Hee Kim

Approved by:



(Chairman) Prof. Han-Lim Lee



(Member) Prof. Jae-Jin Kim



(Member) Prof. Kyung-Soo Han

February 2018

# CONTENTS

<b>CONTENTS .....</b>	<b>I</b>
<b>LIST OF FIGURES .....</b>	<b>III</b>
<b>LIST OF TABLES .....</b>	<b>VII</b>
<b>LIST OF ACRONYMS .....</b>	<b>VIII</b>
<b>1. INTRODUCTION .....</b>	<b>1</b>
1.1. Background .....	1
<b>2. STUDY AREA AND DATA .....</b>	<b>10</b>
2.1. Study Area .....	10
2.2. Satellite Data .....	12
2.3. Auxiliary Data .....	15
2.3.1. Albedo .....	15
2.3.2. Air Temperature .....	17
2.4. Validation Data .....	19
2.4.1. Insolation (INS) ; KMA Pyranometer .....	19
2.4.2. Net Radiation (Rn) ; Eunpyeong Flux tower data .....	19
<b>3. METHODOLOGY .....</b>	<b>22</b>
3.1. Insolation Estimation .....	25
3.2. Net Radiation Algorithm .....	27
3.3. Sensitivity evaluation .....	29
<b>4. RESULTS .....</b>	<b>31</b>
4.1. Insolation (INS) .....	31
4.1.1. Results of Atmospheric Transmittance Model and Hemispherical Integration .....	31
4.1.2. Validation with KMA Pyranometer data .....	34
4.2. Net Radiation .....	38
4.2.1. Retrieval and Analysis of Net Radiation .....	38
4.2.2. Validation with Eunpyeong Flux tower data .....	43

<b>5. SUMMARY AND CONCLUSIONS.....</b>	<b>49</b>
<b>6. REFERENCES .....</b>	<b>51</b>
<b>7. APPEDICES .....</b>	<b>57</b>
7.1. Appendix 1: CMDPS Insolation Algorithm.....	57



# LIST OF FIGURES

Figure 1. The estimated of the annual energy radiation budget of the earth through the climate system.....	7
Figure 2. The schematic diagram expressed net radiation, soil, sensible, and latent heat flux. These elements are in balance.....	8
Figure 3. The schematic diagram expressed trend of net surface radiation by cloud and building at daytime and night. (a) This case shows when clouds and artifacts are not present. In this case of net surface radiation, it has high value in day-time and low value in night-time. (b) This case is the opposite of (a). Net surface radiation has a low value in the day-time and a high value in the night-time.....	9
Figure 4. The study area in this thesis.....	11
Figure 5. (a) COMS Full Disk size and (b) COMS Extend Northern Hemisphere area size image.....	13
Figure 6. Albedo data used in this study. ....	16
Figure 7. One of the air temperature data used in this study. ....	18

Figure 8. The KMA pyranometer location of 3 points and the area of estimated insolation. And the Eunpyeong-gu is located near Seoul point (108).....	20
Figure 9. Scenery image from (a) CNR1 (Kipp&Zonen, Netherlands); (b) north(0°); (c) north-east to east(45-90°); (d) south(180°); and (e) west(270°); and (e) in Eunpyeong Flux tower (Hong, 2014).....	21
Figure 10. Flowchart of this study. ....	24
Figure 11. (a) Result of insolation by Atmospheric Transmittance Model and (b) the result of Hemispherical Integration with a spatial resolution 30 X 30 m. ....	33
Figure 12. Result of correlation analysis between ground insolation (Seoul, Incheon, and Suwon) and (a) COMS Extended Northern Hemisphere daily composite insolation data. And (b) is the result after bias correction of the selected data that is (a).....	35
Figure 13. Time series for observed and estimated INS from COMS Extended Northern Hemisphere at Seoul point (No.108) during 1 year, 2014. The estimated INS is a value that the bias correction is	

applied. The black line is the point insolation data, and the red line is the estimated insolation data..... 37

Figure 14. The land cover and monthly mean net radiation data at the area of this study. (a)The land cover data was reclassified into artificial and vegetation areas. (b) The spatial distribution of net radiation at day time (13:00 KST) and (c) night time (21:00 KST)..... 40

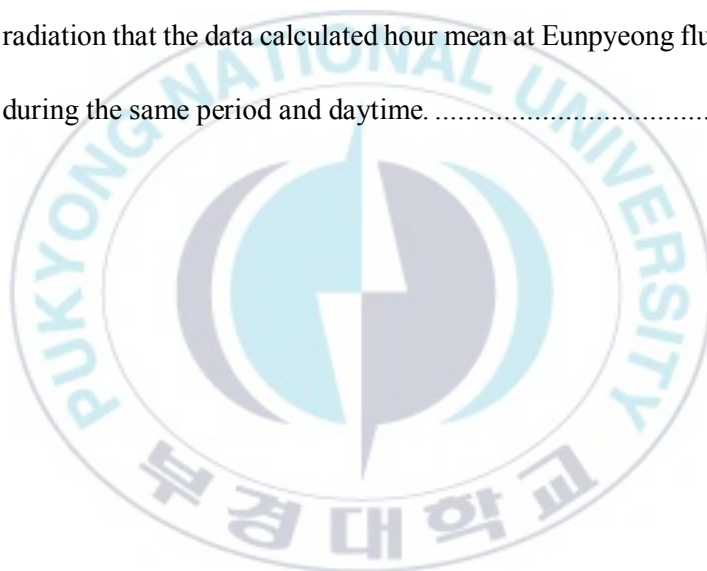
Figure 15. The spatial distribution of net radiation changes during the day, September 4<sup>th</sup>, 2014, which is the area of this study..... 41

Figure 16. The spatial distribution of net radiation changes during the day, September 3<sup>rd</sup>, 2014, which is the area of this study..... 42

Figure 17. Time series for observed and estimated net radiation at Eunpyeong flux tower in Sep. 2014. The black dotted line is the observed and red triangle line is the estimated net radiation data. (upper) The graph is change of net radiation over time during the study period. (below) And the graph at the bottom is the amount of clouds during the study period. The parts of shadow are periods of cloudy or rainy days..... 45

Figure 18. Result of correlation analysis between (a) the observed net radiation data at Eunpyeong flux tower and the estimated net radiation data during the day and (b) during the day time. .... 46

Figure 19. Result of the (a) time series during the study period (Sep. 2014.) and (b) correlation analysis between observed and estimated net radiation that the data calculated hour mean at Eunpyeong flux tower during the same period and daytime. .... 48



## LIST OF TABLES

Table 1. Characteristics of COMS/MI used in the INS algorithm. ....	14
Table 2. Information of 3 points KMA Pyranometer; Seoul, Incheon and Suwon. ....	20
Table 3. The score of correlation analysis between ground insolation (Seoul, Incheon, and Suwon) and daily composite insolation data at each COMS INS area. And the result of previous studies (Jacobs et al.(2002) and Xia et al.(2006)). ....	36
Table 4. The score of correlation analysis between net radiation at flux tower and hourly or hourly mean net radiation data at same pixel. And the result of previous studies (Bisth and Bras (2011) and Ando and Ueyama (2017)). ....	47

## LIST OF ACRONYMS

Acronyms	
ATBD	Algorithm Theoretical Basis Documents
CF	Cloud Factor
CFD	Computational Fluid Dynamics
CLD	Cloud mask
CMDPS	COMS/MI Meteorological Data Processing System
COMS	Communication, Ocean and Meteorological Satellite
ENH	Extended Northern Hemisphere area
INS	Insolation
KMA	Korea Meteorological Administration
LDAPS	Local Data Assimilation and Prediction System
MI	Meteorological Imager
NMSC	National Meteorological Satellite Center
R <sup>2</sup>	Correlation coefficient – squared (R squared)
RMSE	Root Mean Square Error
Rn	Net radiation
Ta	Air Temperature
TBB	brightness temperature
UCM	Urban Canopy Model
VIS	Visible
WV	water vapor

# 위성 원격탐사 기법과 CFD모델 자료를 활용한 도심지에서의 고해상도 지표 순복사 산출

김 홍 희

부 경 대 학 교 대 학 원 공 간 정 보 시 스템 공 학 과

## 요 약

순복사는 증발산량과 같은 지구 순환의 열원으로 사용되는 총 복사 에너지의 총량으로 정의할 수 있으며, 순 장파복사량과 순 단파복사량의 합으로 얻어질 수 있다. 순복사는 저장열, 현열, 잠열과 균형을 이루며, 지표면에서의 다양한 규모의 에너지 분포와 수문학적 순환 과정을 이해하는데 필수적이다. 또한 순복사를 모니터링함으로써 열섬 현상과 도시화 경향을 파악할 수 있다. 이를 위해서는 정확도 높은 순복사가 계산되어야 하며, 연속적이며 높은 공간해상도를 필요로 한다. 따라서 본 연구에서는 위성 자료와 수치모델인 CFD 모델 자료를 이용하여 도시화가 진행 중인 은평구 뉴타운 지역의 고해상도 순복사를 산출 및 모니터링 하고자 한다. 높은 정확도를 가지는 고해상도 순복사를 산출하기 위해서는 순복사에 가장 큰 영향을 미치는 일사량이 정확하게 산출되어야 한다. 이를 위해서 전천을 의미하는 공간적 범위만큼 Hemispherical integration 및 오차 보정을 통해 일사량을 산출하였다. 이 결과를 바탕으로 고해상도 위성기반의 알베도, CFD 모델 기반의 기온을 함께 이용하여 도심지역에서의 고해상도 지표 순복사를 산출하였다. 은평구 플렉스타워 지역에서 관측된 순복사와 비교한 결과, 주 · 야간 전체 RMSE  $54.29 \text{ Wm}^2$ , Bias  $27.42 \text{ Wm}^2$ , 주간 RMSE  $71.12 \text{ Wm}^2$ , Bias  $25.66 \text{ Wm}^2$  의 정확도를 보였으며, 전체적으로 지점 관측 자료와의 유사한 경향을 보였다. 또한 산출된 순복사는 강수와 같은 기상상태를 잘 반영하였으며, 공간적 분포에서 식생 및 인공지물 지역에 대한 순복사의 특징을 잘 나타냈다.

# 1. INTRODUCTION

## 1.1. Background

Net radiation ( $R_n$ ) is the total amount of radiant energy used as a heat source for earth circulation, such as evapotranspiration, in [ $Wm^{-2}$ ]. And also,  $R_n$  is an essential element for understanding the energy distribution and hydrological cycle of the surface (Brutsaert, 1975).  $R_n$  consists of the difference between the radiation incoming into the surface and the outgoing radiation. It can be re-expressed as insolation ( $INS$ ), albedo, and net long-wave radiation.

This can be expressed as :

$$R_n = S \downarrow - S \uparrow + L \downarrow - L \uparrow \quad (1.1.1)$$

$$= R_s \cdot (1 - \alpha) + L \downarrow - L \uparrow \quad (1.1.2)$$

$$= R_s \cdot (1 - \alpha) + R_{nl} \quad (1.1.3)$$

In the above equation (1.1.1),  $R_n$  is net radiation,  $S \downarrow$  and  $L \downarrow$  is incident short-wave and long-wave radiation energy, and  $S \uparrow$  and  $L \uparrow$  is

short-wave and long-wave radiation energy emitted. This can be expressed in terms of INS (**Rs**), albedo (**α**), and net long-wave radiation (**Rnl**) as shown in equation (1.1.2) and (1.1.3). In this regard, Figure 1 shows the average value of the global energy balance, which shows that the amount of radiant energy coming into the surface and the amount of radiant energy emitted are balanced (Trenberth et al., 2009).

$$\mathbf{Rn} = \mathbf{G} + \mathbf{H} + \mathbf{LE} \quad (1.1.4)$$

As in equation (1.1.4), Rn also balances the storage heat flux (**G**), sensible heat flux (**H**), and latent heat flux (**LE**), as shown in Figure 2 (Nouri et al., 2015). At this time, because the change in the energy balance causes the urban heat island effect of the city (Zhao et al., 2014), we need a clear definition of the relationship between the earth and atmosphere in urban area.

In this regard, Rn is used in a various fields, such as input data for the model of evapotranspiration, agriculture, climate monitoring, and weather forecasting (Guoshui et al., 2011; Lima et al., 2012). At this time, evaporation takes charge of maintaining global energy circulation and radiative equilibrium by transporting water vapor to the atmosphere in the

form of latent heat. Therefore, it affects the global climate system and plays a decisive role in determining the characteristics of surface vegetation.

The equation for obtaining evapotranspiration is as follows.

$$\mathbf{ET} = \mathbf{Rn} - \mathbf{B} \cdot (\mathbf{T_s} - \mathbf{T_a}) \quad (1.1.5)$$

Where **ET** is evapotranspiration, **B** is the coefficient required for evapotranspiration calculation. And **Ts** is surface temperature and **Ta** is air temperature. In the above equation, we can see that the Rn consists of one term. This means that Rn is an integral part of the continuous monitoring of evapotranspiration, and Rn also requires constant monitoring. In other words, it is necessary to accurately calculate and monitor of Rn in order to understand the impacts on various fields such as surface energy and climate.

Rn can be described in terms of weather conditions and land type (Figure 3). In the clear sky without clouds or the land type that no artificial materials such as asphalt and concrete, during the day, the surface Rn is high because there is no obstacles exist to block the short-wave radiation(INS), And in the case of night-time, the surface Rn has a low value according to the impossibility of storing the heat. Conversely, in the

cloudy sky or the land type that artificial materials, during the day, the  $R_n$  is lower value by blocking the INS incident upon the cloud, and in the case of night, the  $R_n$  is high due to the radiation does not escape into space by clouds and the high heat storage ratio of artificial materials (Anandakumar, 1999; Asaeda and Ca, 2000; Grimmond, 2007).

According to the UN 2015, in 2050, 66% of those living in city are about to come. This can lead to the same effects as the heat island effect due to temperature rise (Fifth Assessment Report, IPCC).

In addition, according to Zhao et al.(2014) and Hu et al.(2017), the economic development and urbanization accelerated since the second half of the 20<sup>th</sup> century, with an increase in the artificial elements such as roads, buildings. This causes albedo to decrease and surface roughness and heat discharge increased. Therefore, it is difficult to grasp the accurate energy balance due to artificial heat in the city (Roth, 2000), and heat island can cause problems such as smog phenomenon and tropical night phenomenon (Grimmond et al., 2007). So, it is necessary to compare the spatial effects of the urban complex topography, low- and high-rise buildings, and the tendency of time series with the point data in order to understand and monitor the distribution and circulation of the surface energy in urban areas.

In this regard, computation or research related to Rn was actively conducted in the related conditions such as the clear sky, top of atmosphere, vegetation, etc. Recently, Rn estimation and monitoring, which mainly targets urban area was actively underway. Before the 2000s, research on Rn related to conditions such as clear sky, top of atmosphere, and various land cover type. In the 2000s, a combination of satellite and energy balance models led to Rn research on various land cover type. After 2010s, many researches related to Rn have been carried out by combining models related to energy balance in urban areas such as USA, Singapore, Japan, and China.

Ohring and Clapp (1980), Alados et al. (2003), Wang and Liang (2008), Zhao et al. (2014), Pan et al.(2015), Hu et al. (2017) and Picón et al. (2017) used polar orbiting satellite data such as Moderate Resolution Imaging Spectroradiometer (MODIS), LANDSAT to estimate Rn in various areas such as the clear sky, urban and suburban areas, and tropical regions. And they also used albedo to account for the amount of cloud and explained the phenomenon of heat island through Rn. However, this has the disadvantage that the time continuity of the output is inferior.

Harshan et al. (2017) also estimated and compared Rn using Town Energy Balance (TEB) model in Singapore, but the model is an urban model, there is a limitation that it does not reflect the height difference of

the building. As mentioned above, although there have been a number of  $R_n$  calculations through the combination of satellite and energy balance model, study to calculate  $R_n$  through the fusion of data based on satellite and Computational Fluid Dynamics (CFD) model which is the method to be tried in this study has not been conducted national and international.

It means that urbanization and interest in the phenomenon of city is increasing in many areas to active monitoring, calculation and analysis of  $R_n$  using satellite data centering on urban areas. And it can judge urban heat island phenomenon and urbanization tendency as well as grasp energy distribution in city center through  $R_n$ . Therefore, complex terrain and spatial effects should be considered to understand the energy distribution and circulation of the surface in urban areas. And it was also determined that a high spatial resolution and continuous  $R_n$  computation are required.

In addition, if the model is used, data can be calculated according to the spatial resolution desired by the user, but there is a disadvantage that it takes much time to process the data depending on the server environment. If the satellite is used, user can't obtain high accurate data due to the absence of observation data or cloud. But there is an advantage that it is possible to observe instantly using satellite, the ability to acquire data in a wide area, and the calculation of  $R_n$  in non-access areas.

Therefore, in this study, we calculate high-resolution  $R_n$  in urban areas using Communication, Ocean and Meteorological Satellite (COMS) and Landsat-8 to improve the disadvantages of spatial and temporal resolution, and CFD model that reflects the height of the building.

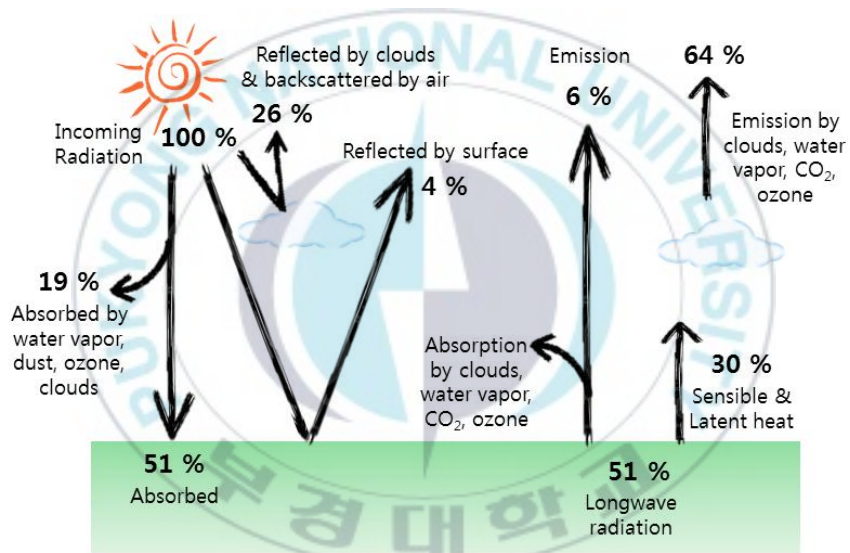


Figure 1. The estimated of the annual energy radiation budget of the earth through the climate system.

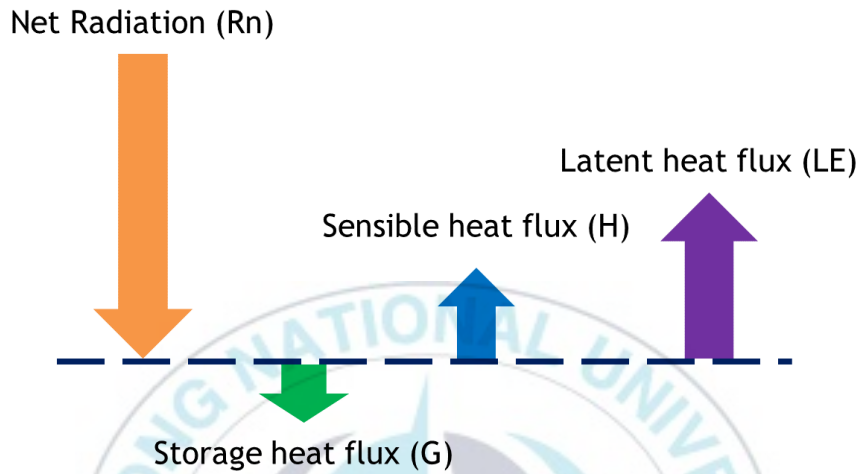


Figure 2. The schematic diagram expressed net radiation, soil, sensible, and latent heat flux. These elements are in balance.

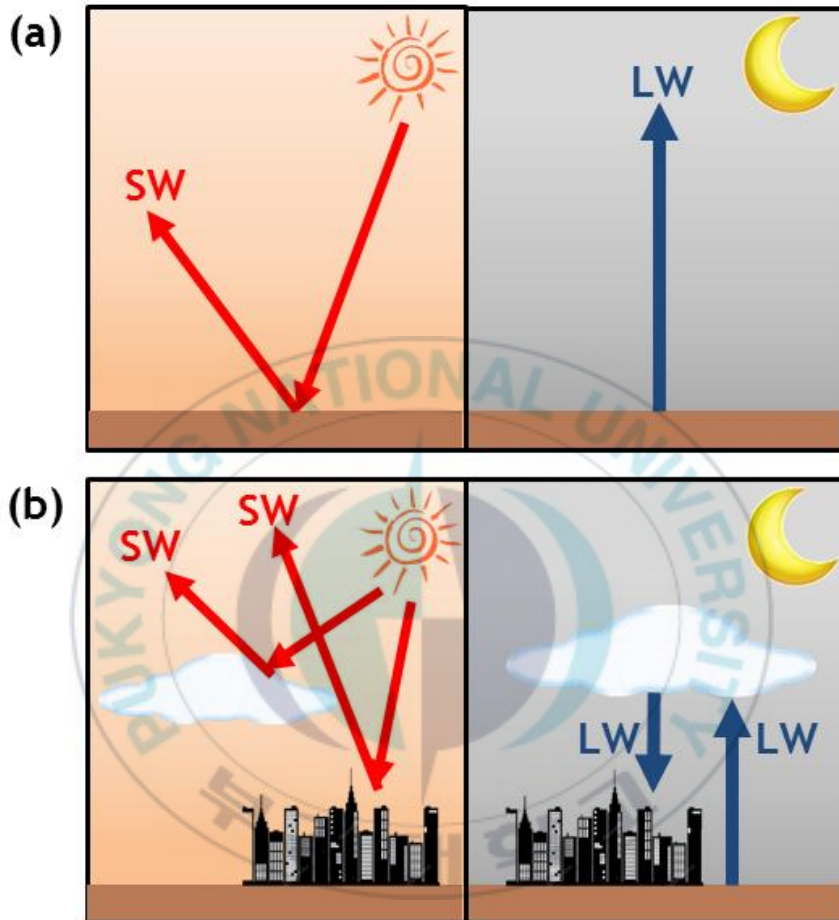


Figure 3. The schematic diagram expressed trend of net surface radiation by cloud and building at daytime and night. (a) This case shows when clouds and artifacts are not present. In this case of net surface radiation, it has high value in day-time and low value in night-time. (b) This case is the opposite of (a). Net surface radiation has a low value in the day-time and a high value in the night-time.

## 2. STUDY AREA AND DATA

### 2.1. Study Area

The study area of this study is in Seoul, Korea between 37.63°N and 37.64°N and 126.92°E and 126.93°E (Figure 4). This area corresponds to the area of 1 km X 1 km from the flux tower (37.6351°N, 126.9293°E) of Eunpyeong-gu, Seoul. And also, this is the area where urbanization is going on and including various land type such as broad-leaf forest, Grassland, Building, road, etc. It is appropriate to calculation and analysis of Rn. And the period of this study is 1 month from 1st September to 30th September 2014. This period include various climate statuses such as sunny, cloudy, or rainy.

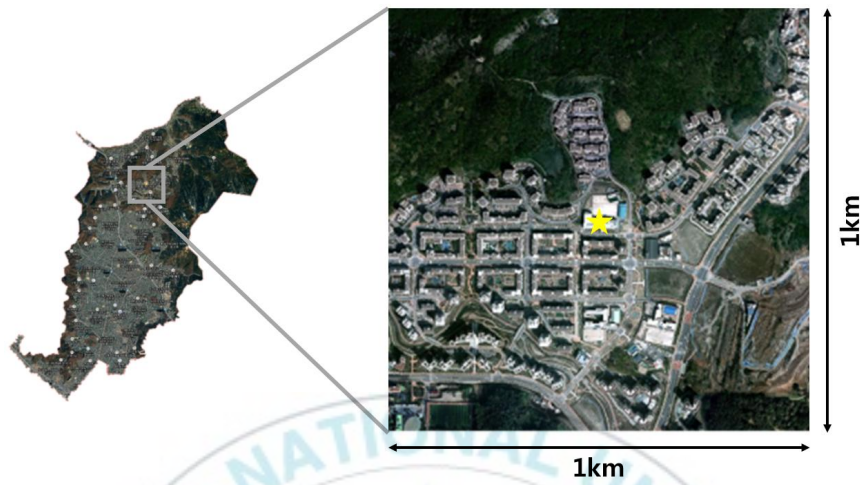


Figure 4. The study area in this thesis.

## 2.2. Satellite Data

COMS / Meteorological Imager (MI) is the first multipurpose geostationary satellite developed with Korea technology. The COMS / MI is launched on June 27<sup>th</sup>, 2010 and it is a satellite that serves as communication, marine observation and meteorological satellites. It is at a longitude of 128.2°E and altitude of 3600 km from the Earth's equator that the COMS / MI always observes from the same angle of view. Figure 5 shows the area provided by the COMS / MI. It is divided into Full Disk, Extended Northern Hemisphere area (ENH), East Asia, and Korea.

In this study, we used ENH data. ENH observes 96 times a day from 00:00 UTC with a temporal resolution of 15 minutes. For the ENH region, this study used timely data with a temporal resolution of 1 hour.

The COMS / MI sensor consists of five spectral channels of Level 1B data; visible (VIS), short-wave infrared (SWIR), water vapor (WV) and infrared channel-1 and -2 (IR1 and IR2). The center wavelengths of these are 0.6  $\mu\text{m}$ , 3.7  $\mu\text{m}$ , 6.7  $\mu\text{m}$ , 10.8  $\mu\text{m}$  and 12  $\mu\text{m}$ , respectively. In the case of spatial resolution, the remaining channels except the visible channel are 4 X 4 km and the visible channel is 1 X 1 km. This is shown in Table 1.

In this study, we use cloud mask (CLD) and Cloud Factor (CF) data to analyze the effect of cloud, which is a measure of the degree of attenuation due to clouds. CF referenced COMS/MI Meteorological Data Processing System Insolation Algorithm Theoretical Basis Documents (CMDPS INS ATBD, 2012).

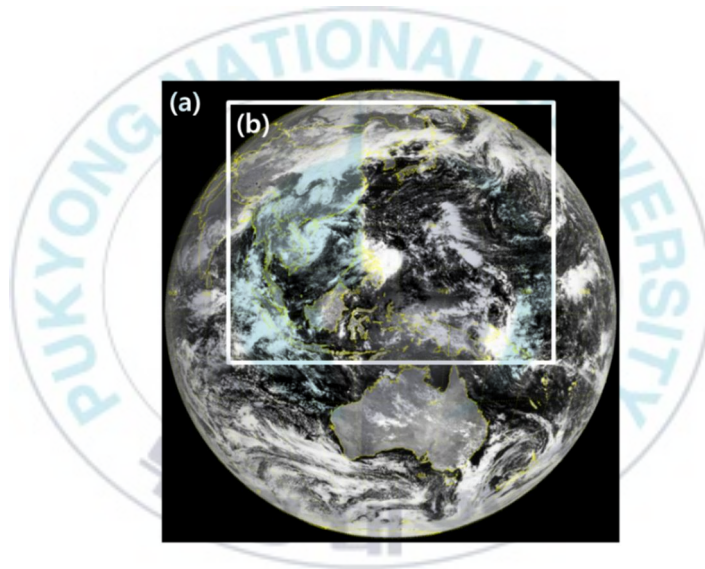


Figure 5. (a) COMS Full Disk size and (b) COMS Extend Northern Hemisphere area size image.

Table 1. Characteristics of COMS/MI used in the INS algorithm.

Channel	Center Wavelength (μm)	Spatial Resolution (km)	Used in this study
Level 1B	VIS	0.67	0
	SWIR	3.7	4 X 4
	WV	6.7	4 X 4
	IR1	10.8	4 X 4
	IR2	12.0	4 X 4
Level 2	CLD	4 X 4	0

## **2.3. Auxiliary Data**

### **2.3.1. Albedo**

Albedo is one of the major climate variables that determine the absorption of solar energy and is an important variable in climate change research. The albedo data used in this study is recorded on September 19<sup>th</sup>, 2014. And it is a broadband albedo based on Landsat-8 satellite calculated by Lee et al. (2016). The spatial resolution of this data is 30 X 30 m and the temporal resolution is 16 days. This data has an accuracy of RMSE 0.003,  $R^2$  0.89. In the  $R_n$  calculation, albedo has the greatest effect on day-time.

The reason why there is one consistent data in this study period is that the cloud mask provided by Landsat is used to eliminate the error caused by the cloud, and the albedo is calculated for observation days that can minimize the cloud effect. Therefore, the albedo data used in this study is the data on September 19<sup>th</sup>, 2014, which corresponds to the period of this study, and the spatial distribution of albedo corresponding to this date is shown in Figure 6. In this, the empty part of the data is the cloud exists.

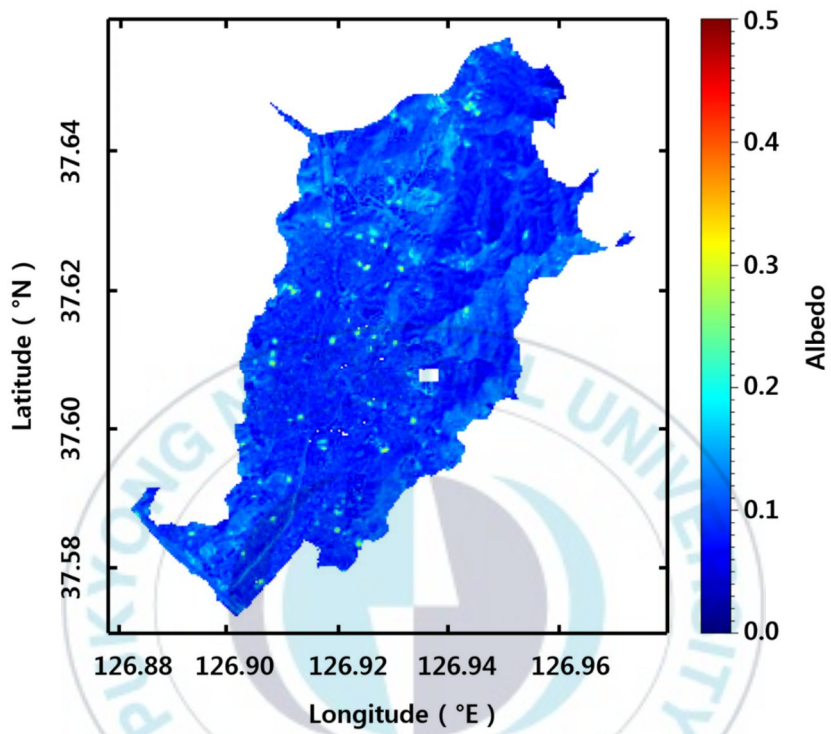


Figure 6. Albedo data used in this study.

### **2.3.2. Air Temperature**

Air Temperature ( $T_a$ ) is one of the climate variables that mean the temperature of the atmosphere. According to Hanna et al. (2009), changes in land cover due to urban development and growth increase the heat flux and  $T_a$  in urban areas. Given this,  $T_a$  is also an important variable in climate change research.

The  $T_a$  data period and area used in this study is equal of this study, and the  $T_a$  data based on the CFD model (Kang and Kim, 2017; Figure 7). The spatial resolution is 10 X 10 m and the temporal resolution (integration time) is 1 hour. This data has an accuracy of RMSE 1.252 °C. In the  $R_n$  calculation,  $T_a$  has the greatest effect on night-time when the INS and albedo are excluded.

The CFD model is drive using surface temperature based on Urban Canopy model (UCM), potential temperature, and wind components based on Local Data Assimilation and Prediction System (LDAPS) in the east-west, north-south directions and simulates turbulent kinetic energy, temperature, and wind components in the east-west, north-south, and vertical distribution.

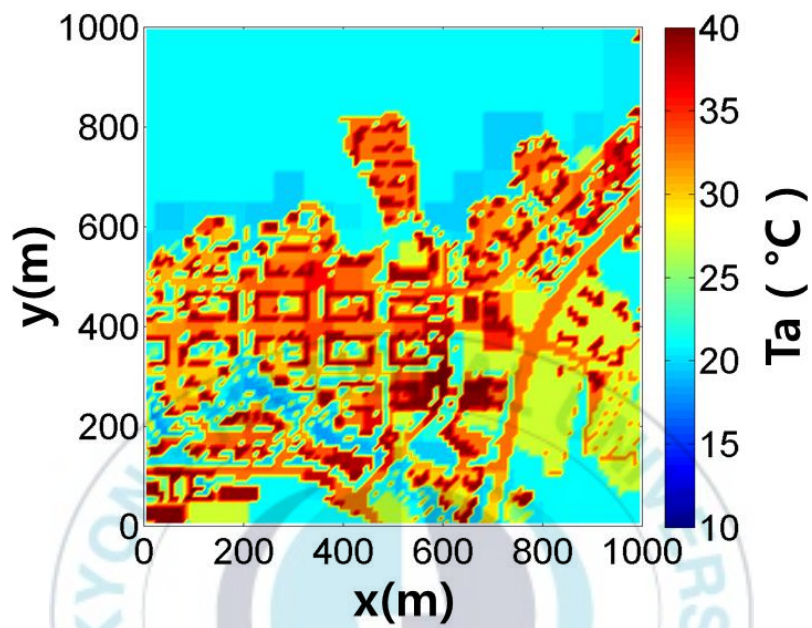


Figure 7. One of the air temperature data used in this study.

## **2.4. Validation Data**

### **2.4.1. Insolation (INS) ; KMA Pyranometer**

In this study, the pyranometer data for validation of INS and it is the same period of the INS. We used for 3 points data that Seoul, Incheon and Suwon of 37 stations of the Korean Peninsula provided by the Korea Meteorological Administration (KMA). The pyranometer data is made at 2-minute intervals and average hourly values are given as representative values. The information of the ground observation points used in this study is as follows (Table 2, Figure 8).

### **2.4.2. Net Radiation (Rn) ; Eunpyeong Flux tower data**

In this study, the observation data for Rn validation is located at the flux tower site in Eunpyeong-gu, Seoul, and the period is same as the Rn calculation period. This data is an average observation for 1 hour, and a flux-measurement lattice tower of 10 m height is set up the net radiometer on the rooftop of a building of 20 m height. In other words, it is installed at a total height of 30m from the ground. The net radiometer installed on the rooftop of the building is CNR1 (Kipp & Zonen B.V.), which measures the radiation velocity of upward and downward flux (Hong et al., 2016; Figure 9).

Table 2. Information of 3 points KMA Pyranometer; Seoul, Incheon and Suwon.

No.	Name	Latitude(°N)	Longitude(°E)
108	Seoul	37.5714	126.9657
112	Incheon	37.4777	126.6240
119	Suwon	37.2723	126.9853

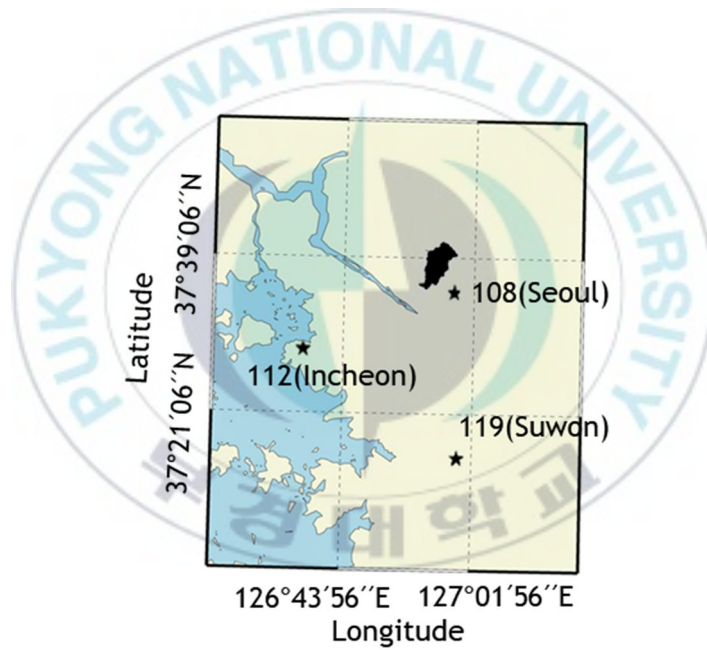


Figure 8. The KMA pyranometer location of 3 points and the area of estimated insolation. And the Eunpyeong-gu is located near Seoul point (108).

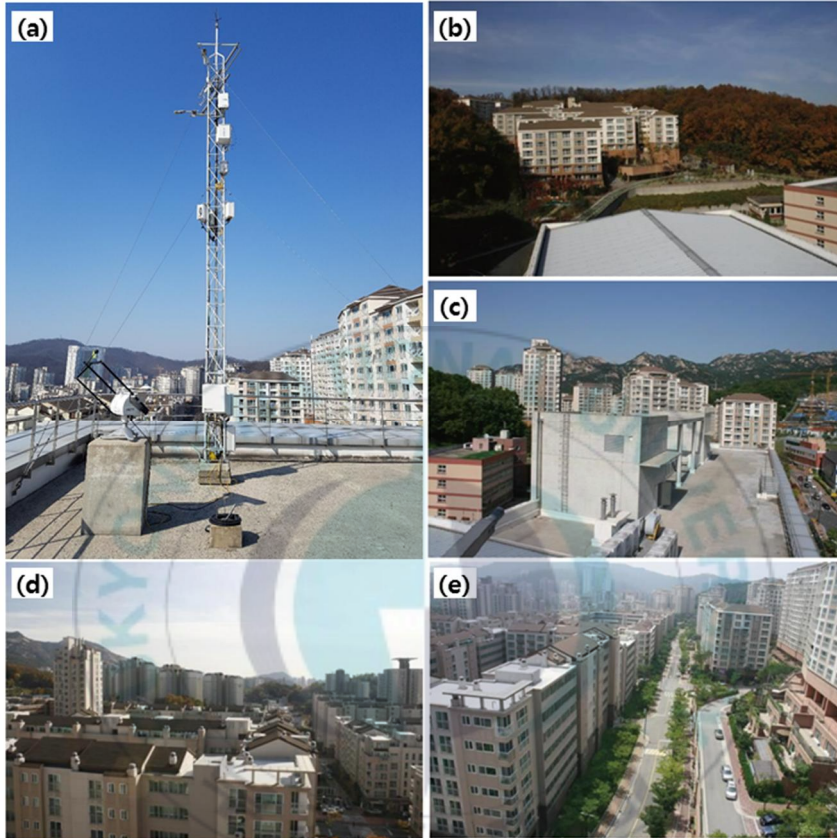


Figure 9. Scenery image from (a) CNR1 (Kipp&Zonen, Netherlands); (b) north( $0^\circ$ ); (c) north-east to east( $45\text{-}90^\circ$ ); (d) south( $180^\circ$ ); and (e) west( $270^\circ$ ); and (e) in Eunpyeong Flux tower (Hong, 2014).

### 3. METHODOLOGY

Figure 10 is a flow chart of this study. We first determine the accuracy of the INS (PART A) and then retrieval the Rn (PART B).

First is PART A. It is the step of calculating the INS before retrieval the Rn. According to Heitor et al.(1991), INS is a major component of Rn. And INS is the most influential factor of the day-time with albedo when calculating Rn. Therefore, the INS must also be accurately calculated to produce an accurate Rn. In this step, we calculate the INS using the Atmospheric Transmittance Model. After this step, INS has a spatial resolution of 30 X 30 m. After that, we performed Hemispherical Integration for a radius of 24km, which means the whole area. And then, we validated the estimated INS data with the observations data and performed the bias correction for more accurate Rn calculation. Further details are given in section 3.1.

The following is PART B. It is the part that retrieval the Rn using the continuous and high resolution INS amount calculated from PART A. In this section, we retrieval the Rn in the urban area using the simulated Ta value through CFD model and albedo calculated by Landsat-8 satellite. Repeating the above, when calculating Rn, INS and albedo are the most influential factor in the day-time, and Ta is the most influence in the night-

time. For the  $R_n$  calculation, the Idso, S. B., and Jackson, R. D.(1969), Wright, J. L.(1982) formula is used. Based on these results, we validate the data with the Eunpyeong flux tower data. Further details are given in section 3.2.



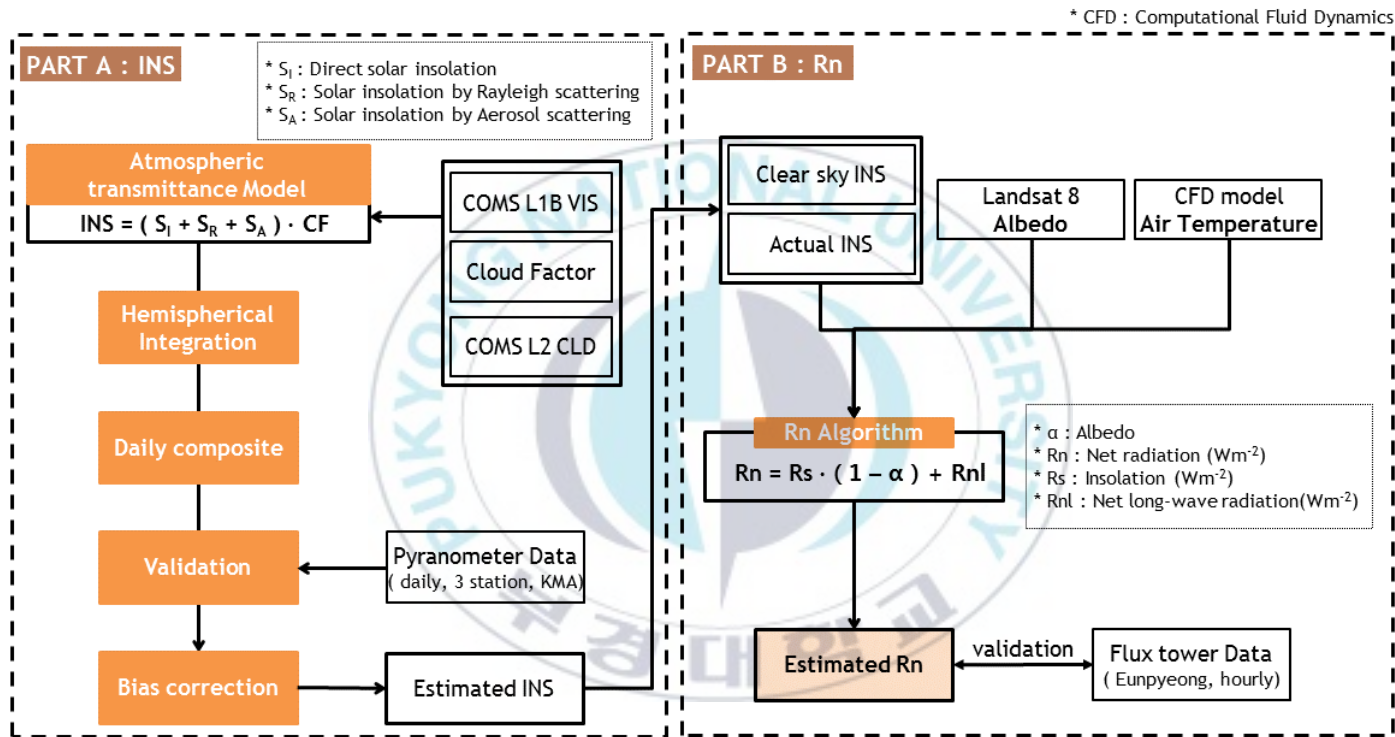


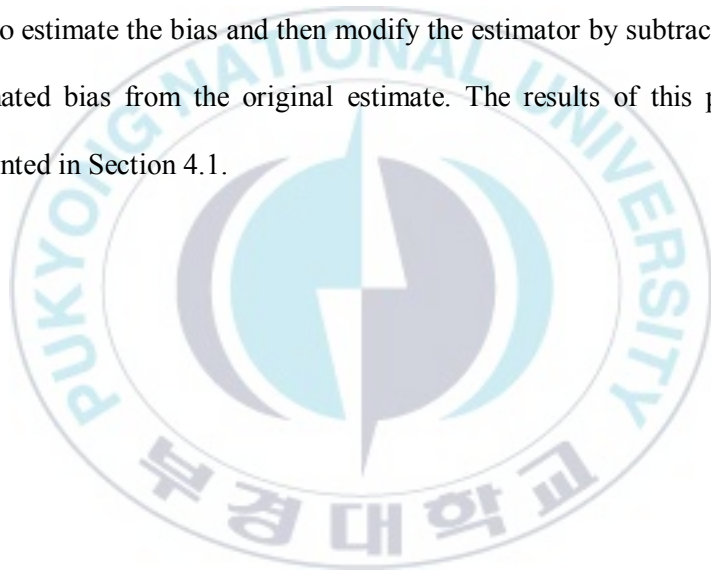
Figure 10. Flowchart of this study.

### 3.1. Insolation Estimation

In order to calculate the accurate INS, we compared the INS calculated using COMS provided ENH. Here, the reason for directly calculating without using the INS data provided by KMA is that there is a problem in the unit of ozone input when calculating the INS dose in the case of the INS amount provide by the existing KMA. Therefore, in this study, the unit of ozone was modified without using the existing INS, and the INS corresponding this study period was calculated by the Atmospheric Transmittance Model using COMS Meteorological Data Processing System (CMDPS) INS algorithm. The estimated INS generated by the CMDPS INS algorithm is obtained by sum of direct INS and scatter INS. If there is a cloud, the INS is multiplied by CF when calculate the INS. The detailed methods and coefficients for INS using the CMDPS INS algorithm is available in Appendix 1: CMDPS Insolation Algorithm.

Next, we performed Hemispherical Integration. And then, we conducted daily mean of each data for direct comparison with the observation data of INS. In this study, it was difficult to validation the INS as the area of  $R_n$ . So, the area of calculation of the INS was included  $R_n$  area and 3 points; Seoul, Incheon and Suwon (Figure 8). In order to confirm that the output is continuous, one year was selected as the INS

calculation period from January 1st, 2014 to December 31th, 2014 including the study period. And we compared the accuracy of the combined the daily mean INS data with the temporal resolution of 1 hour intervals. Because there is no INS at night, there is up to 12 data at 1 hour intervals depending on the time resolution. As a result of the validation, we performed the bias correction to improve the accuracy. This method is that to estimate the bias and then modify the estimator by subtracting the estimated bias from the original estimate. The results of this part are presented in Section 4.1.



### 3.2. Net Radiation Algorithm

The Rn calculation algorithm used in this study is Idso, S. B., and Jackson, R. D.(1969), Wright, J. L.(1982), and it is as follows.

$$\mathbf{Rn} = \mathbf{Rs} \cdot (1 - \alpha) + \mathbf{Rnl} \quad (3.2.1)$$

$$\mathbf{Rnl} = \epsilon_{\text{bulk}} \cdot \sigma \cdot T\alpha^4 \quad (3.2.2)$$

$$\epsilon_{\text{bulk}} = - [ (\mathbf{aa} \cdot \mathbf{CR}) + \mathbf{bb} ] \cdot [ \mathbf{a1} + \mathbf{b1} \cdot \mathbf{ea} ] \quad (3.2.3)$$

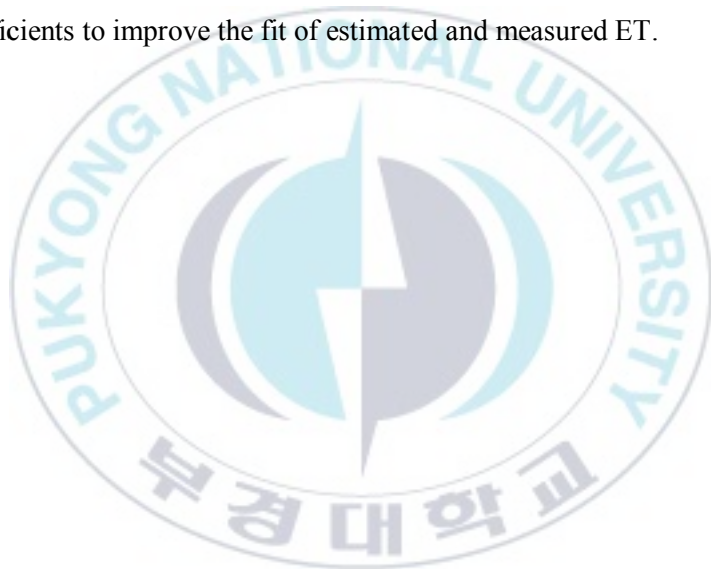
$$\mathbf{ea} = \exp(-7.77 \cdot 10^{-4} \cdot (273 - T\alpha)^2) \quad (3.2.4)$$

Where **Rn** is Net Radiation, **Rs** is INS, and **Rnl** is Net long-wave radiation. **Rn**, **Rns**, and **Rnl** are radiant energy in [MJ m<sup>-2</sup>]. **α** is Albedo, **Ta** is Air temperature in [K]. **ε<sub>bulk</sub>** is a combined emissivity for both the sky and the ground surface. **CR** is Cloudy sky INS / Clear sky INS and it is a dimensionless coefficient. **σ** is Stefan-Boltzmann constant ( 4.7 X 10<sup>-9</sup> MJ m<sup>-2</sup>K<sup>-4</sup> ), **ea** is actual vapor pressure of the air in [kPa]. **a1, b1, aa, bb** are experience coefficients.

The Stefan-Boltzmann equation is that the sum of the light energy of all the wavelengths emitted from a unit surface area of a black body is

proportional to the fourth power of the black body Kelvin temperature. The equation is used to determine of the radiant heat transfer is used to determine the  $R_{nl}$ . And  $\epsilon_{bulk}$  is an alternated method of estimation  $R_{nl}$  when humidity data is not available. It was developed by Idso and Jackson(1969).

Wright(1982) introduced a model that estimates  $R_n$  by adding variable coefficients to improve the fit of estimated and measured ET.



### 3.3. Sensitivity evaluation

The performance of INS and Rn is evaluated against the observations at the flux sites by the statistical techniques. The root-mean-square error (RMSE) is commonly used measure when the difference between the observed value in real environment and estimated value. This is suitable for expressing precision. Each difference value is also known as a residual.

$$\mathbf{RMSE} = \left[ \frac{\sum_{i=1}^n (y_i - x_i)^2}{n} \right]^{0.5} \quad (3.3.1)$$

Where  $(x_i - y_i)$  represents the difference between the observed  $x$  and simulated  $y$  flux term at each hourly or daily interval  $\mathbf{I}$ ,  $\mathbf{n}$  represents the total number of hours or daily.

The bias measures how the estimated value deviated from its observed value and is displayed if there is underestimation or overestimation. If the bias value is positive, this means that the estimated value is overestimation.

$$\mathbf{bias} = \left[ \frac{\sum_{i=1}^n (y_i - x_i)}{n} \right] \quad (3.3.2)$$

In statistic, Correlation coefficient ( $R^2$ ) is used as the strength to determine the degree of similarity or correlation between the estimated and the measured value. For  $R^2$ , it has a value between 0 and 1. If the  $R^2$  is zero, then the relationship between the two variables is irrelevant. Conversely, if the correlation of two variables is high, it has a value close to 1.

$$R^2 = \left[ \frac{\sum_{i=1}^n (x_i - \bar{x})(y_i - \bar{y})}{\sqrt{\sum_{i=1}^n (x_i - \bar{x})^2} \sqrt{\sum_{i=1}^n (y_i - \bar{y})^2}} \right]^2 \quad (3.3.3)$$

Where  $\bar{x}$  and  $\bar{y}$  are each an average of observed and estimated value.

## 4. RESULTS

### 4.1. Insolation (INS)

#### 4.1.1. Results of Atmospheric Transmittance Model and Hemispherical Integration

Figure 11 shows the spatial distribution of the results of the Atmospheric Transmittance Model and Hemispherical Integration processes, and it is the result of January 1, 2014. It shows that the distributions of the values are generally similar through the INS calculated by the Atmospheric Transmittance Model (Figure 11 (a)) and the Hemispherical Integration (Figure 11 (b)) with a spatial resolution of 30 X 30 m. In Figure 11 (a), we notice that the difference between nearby pixels is noticeable, and we can see that the difference between adjacent pixels shown in Figure 11 (b) decreases. Also, the overall spatial distribution of Figure 11 (a) and (b) did not show much difference, and the spatial distribution of the INS according to the land-sea type and the time can be understood.

In addition, before performing validation with pyranometer data, we perform daily averaging to match the temporal resolution on both data that estimated and pyranometer INS data. At this time, when daily average is

performed, if there is no observation of the solar transit time during one observation time, the daily average calculation value may be calculated to be lower in this part.



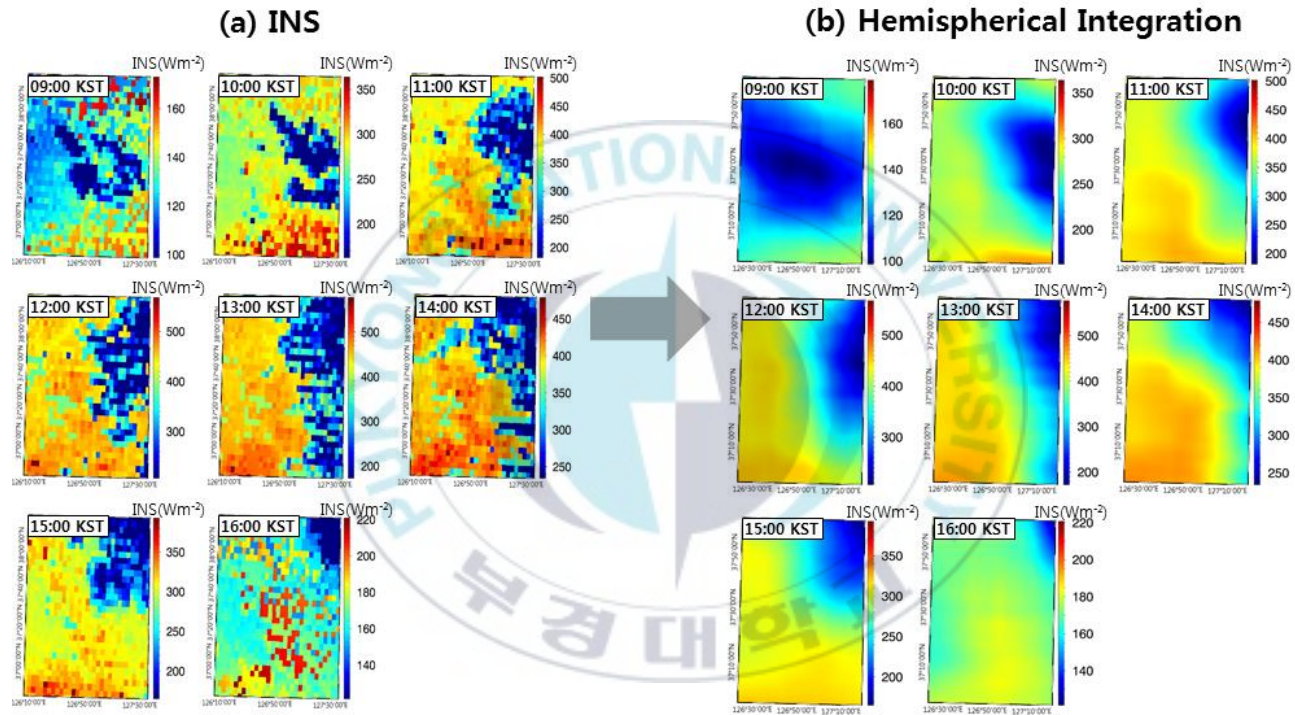


Figure 11. (a) Result of insolation by Atmospheric Transmittance Model and (b) the result of Hemispherical Integration with a spatial resolution 30 X 30 m.

#### 4.1.2. Validation with KMA Pyranometer data

We produced comparatively continuous data for continuous Rn computations. Figure 12(a) is the result of comparing the estimated INS with the pyranometer data at ground observation points in Seoul, Incheon and Suwon. The data showed RMSE  $36.10 \text{ Wm}^{-2}$ , Bias  $20.07 \text{ Wm}^{-2}$ , and Slope 1.00. Figure 12 (b) is the result of the bias correction of the selected INS data for more accurate Rn calculation. The result are RMSE  $29.94 \text{ Wm}^{-2}$ , Bias  $-1.14\text{E}^{-4} \text{ Wm}^{-2}$ . This score is more accurate than RMSE  $46 \text{ Wm}^{-2}$ , which is the result of the calculation of Geostationary Operational Environmental Satellite (GOES) data (Jacobs et al., 2002), and close to RMSE  $25 \text{ Wm}^{-2}$ , which is the result of calculation of National Centers for Environmental Prediction (NCEP) data (Xia et al., 2006) (Table 3).

In addition, Figure 13 is a time series graph showing the Figure 12 (b). This graph showing the INS calculated based on COMS and the measured value of INS at ground observation point in Seoul. The black line is the measured INS data, and the red line is the estimated INS data. It was confirmed that the estimated INS data in the time series graph follows the tendency of the measured INS data basically. The estimated INS data is continuous, and it is judged that the calculation in this process can be used to produce high resolution Rn.

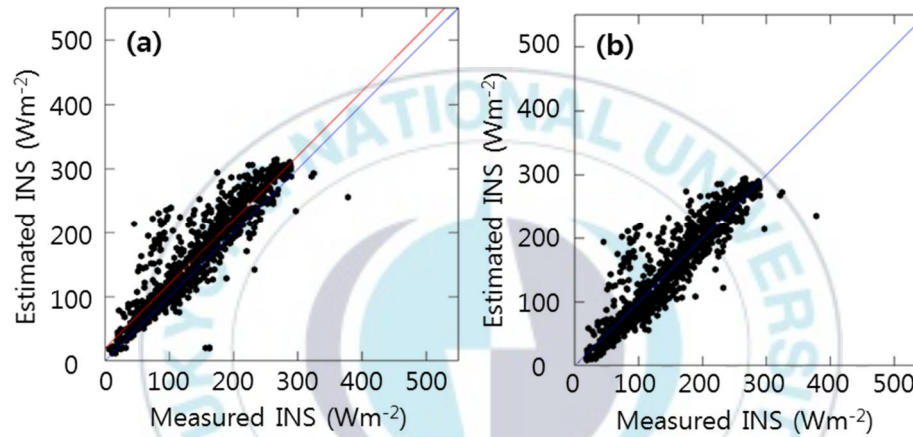


Figure 12. Result of correlation analysis between ground insolation (Seoul, Incheon, and Suwon) and (a) COMS Extended Northern Hemisphere daily composite insolation data. And (b) is the result after bias correction of the selected data that is (a).

Table 3. The score of correlation analysis between ground insolation (Seoul, Incheon, and Suwon) and daily composite insolation data at each COMS INS area. And the result of previous studies (Jacobs et al.(2002) and Xia et al.(2006)).

DATA		RMSE(Wm <sup>-2</sup> )	Bias(Wm <sup>-2</sup> )	Slope	
COMS	(a)	Extended Northern Hemisphere	36.10	20.07	1.00
	(b)	Bias correction of the (b)	29.94	-1.14E <sup>-4</sup>	1.00
GOES		Jacobs et al. (2002)	46.	-	-
NCEP		Xia et al. (2006)	25.	-	-

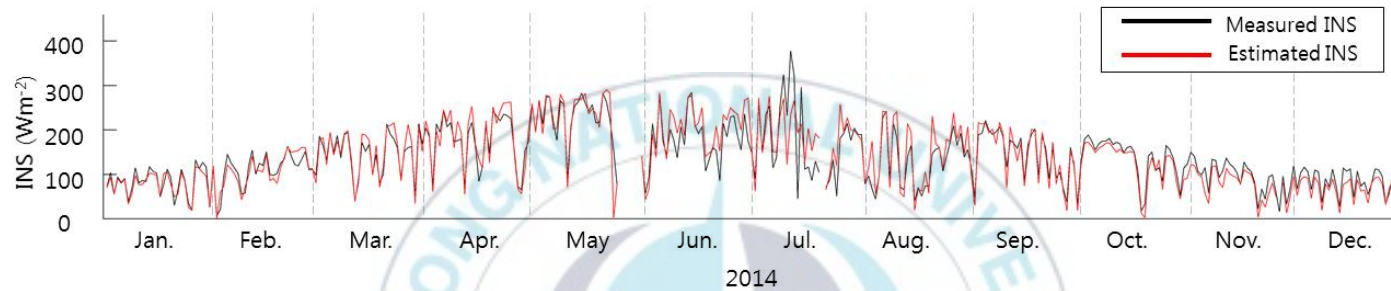


Figure 13. Time series for observed and estimated INS from COMS Extended Northern Hemisphere at Seoul point (No.108) during 1 year, 2014. The estimated INS is a value that the bias correction is applied. The black line is the point insolation data, and the red line is the estimated insolation data.

## 4.2. Net Radiation

### 4.2.1. Retrieval and Analysis of Net Radiation

R<sub>n</sub> calculated in this study has a spatial resolution of 30 X 30 m and a temporal resolution of 1 hour according to the data used in the calculation. Before quantitative analysis of R<sub>n</sub>, spatial distribution of R<sub>n</sub> according to vegetation and artificial area was analyzed.

Figure 14 shows the average monthly R<sub>n</sub> for the month of September at 13 KST and 21 KST, representing the map of the land cover and day- and night-time. Land cover map is middle classification level scale of 1:25,000 that obtained from the Ministry of Environment. We followed the classification system included in the study area, and classified urban area and roads as artifacts (Figure 14 (a)). In the case of day-time, artifact area (School, Fluxtower, Building, and Road) was relatively lower than that of vegetation area (broadleaf forest, Grassland, and Mixed forest) (Figure 14 (b)). Conversely, in the case of night-time, artifacts area were higher than vegetation area. This is due to the difference in R<sub>n</sub> as a result of the interception of the incoming and outgoing radiation depending on the existence of artifacts (Grimmond, 2007). And, In general, albedo is higher in vegetation than the urban area. However, due to the recent industrial development of the urban area and the increase of automobile

soot, factors such as aerosol are increasing, and the solar radiation is scattered and reflected by factors. As a result, albedo is higher in the urban than the vegetation area. Therefore, in the case of the day-time when the influence of INS and albedo is higher than the air temperature, the value of Rn is lower in the urban than the vegetation area. At night-time, the air temperature that has a great influence on the contrary to the day-time is higher in the urban than the vegetation area. Therefore, the Rn of the urban area is higher than the vegetation area at the night-time where the influence of the temperature is great.

Figure 15 shows the spatial distribution of Rn changes during the day, September 4<sup>th</sup>, 2014, which is calculated using the INS based on COMS, the Albedo based on Landsat-8, and the Ta based on CFD model. The range of fluctuation from a minimum of about  $-20 \text{ Wm}^{-2}$  to a maximum of about  $570 \text{ Wm}^{-2}$ , indicating that day-to-day fluctuations in Rn in urban area are significant. And also, Figure 15 and Figure 16 shows the Rn change during the day on September 4<sup>th</sup> and 3<sup>rd</sup>, 2014, showing the relationship between Rn and Ta. Overall, in this Figure, artifact area is low than vegetation area at day-time, and it shows opposite trend at night-time. For example, daily Ta range that the difference between the maximum and minimum Ta during the day, on cloudy days, clouds block the INS. So the surface is not easily heated, and the water vapor stores a lot of heat in the

air at night. On the other hand, on a clear day when the humidity is low in the air, the terrestrial radiation energy is easily transferred to the atmosphere. At night, it can't hold heat, so it cools rapidly and the day-to-day difference increases. Thus, Figure 15 shows a clear day in which the  $R_n$  during the day decreases from about  $58 \text{ Wm}^{-2}$  to about  $635 \text{ Wm}^{-2}$ , and at night, to a value similar to the  $R_n$  on cloudy day. This shows that there is not much radiant energy in the atmosphere compared to cloudy days. Conversely, Figure 16 shows a cloudy day that the  $R_n$  during the day changes from about  $8 \text{ Wm}^{-2}$  to about  $74 \text{ Wm}^{-2}$ , and to  $-18 \text{ Wm}^{-2}$  at night. It can be seen that the  $R_n$  from the cloudy day changes to a narrow width with the decreasing  $R_n$ . This shows that there is a lot of radiant energy in the atmosphere.

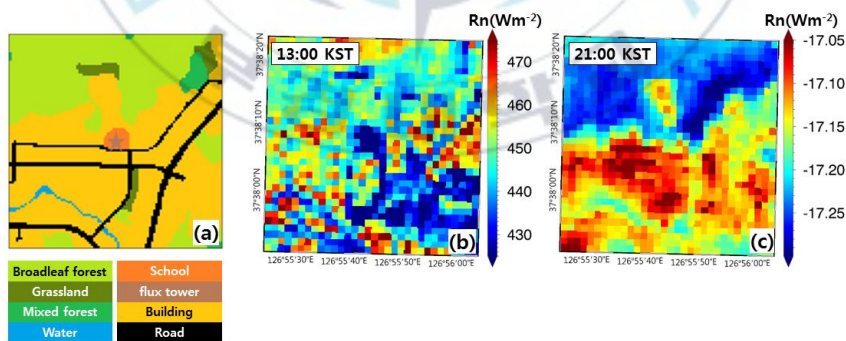


Figure 14. The land cover and monthly mean net radiation data at the area of this study. (a)The land cover data was reclassified into artificial and vegetation areas. (b) The spatial distribution of net radiation at day time (13:00 KST) and (c) night time (21:00 KST).

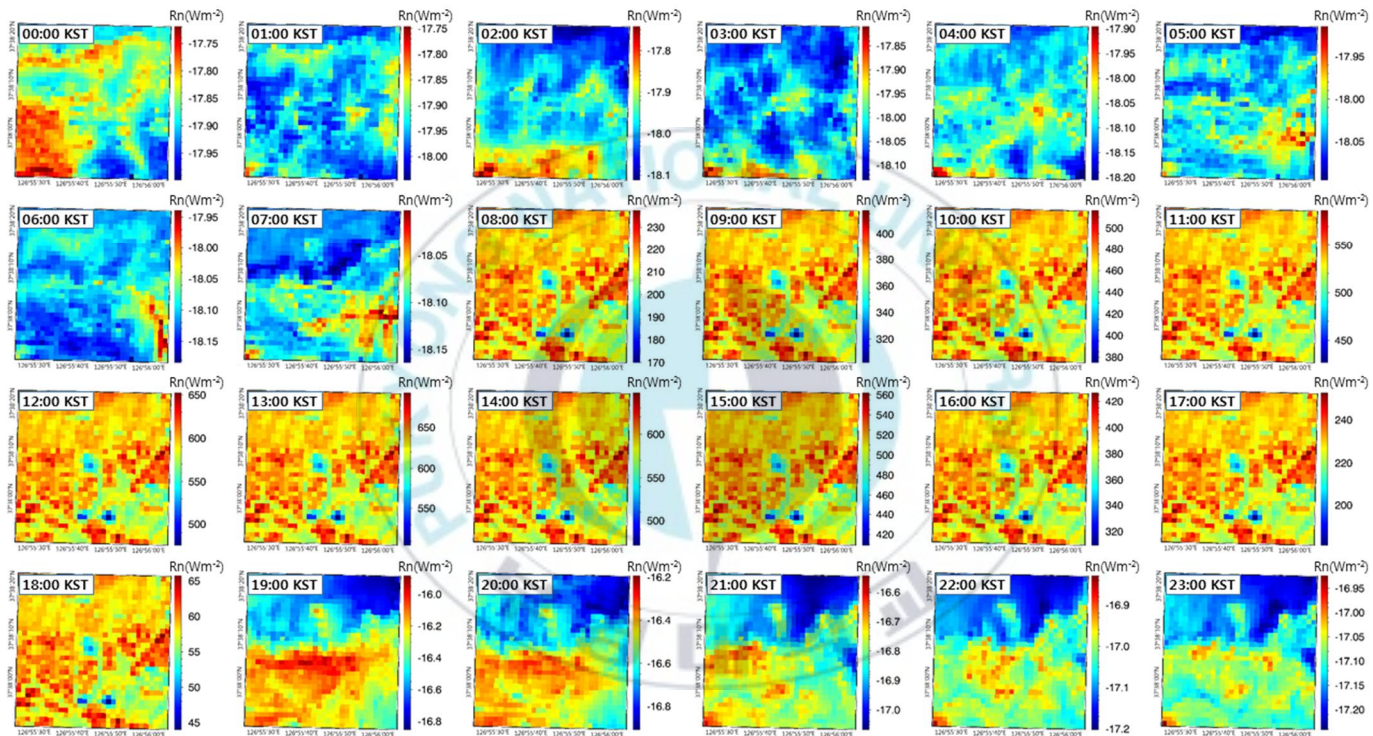


Figure 15. The spatial distribution of net radiation changes during the day, September 4<sup>th</sup>, 2014, which is the area of this study.

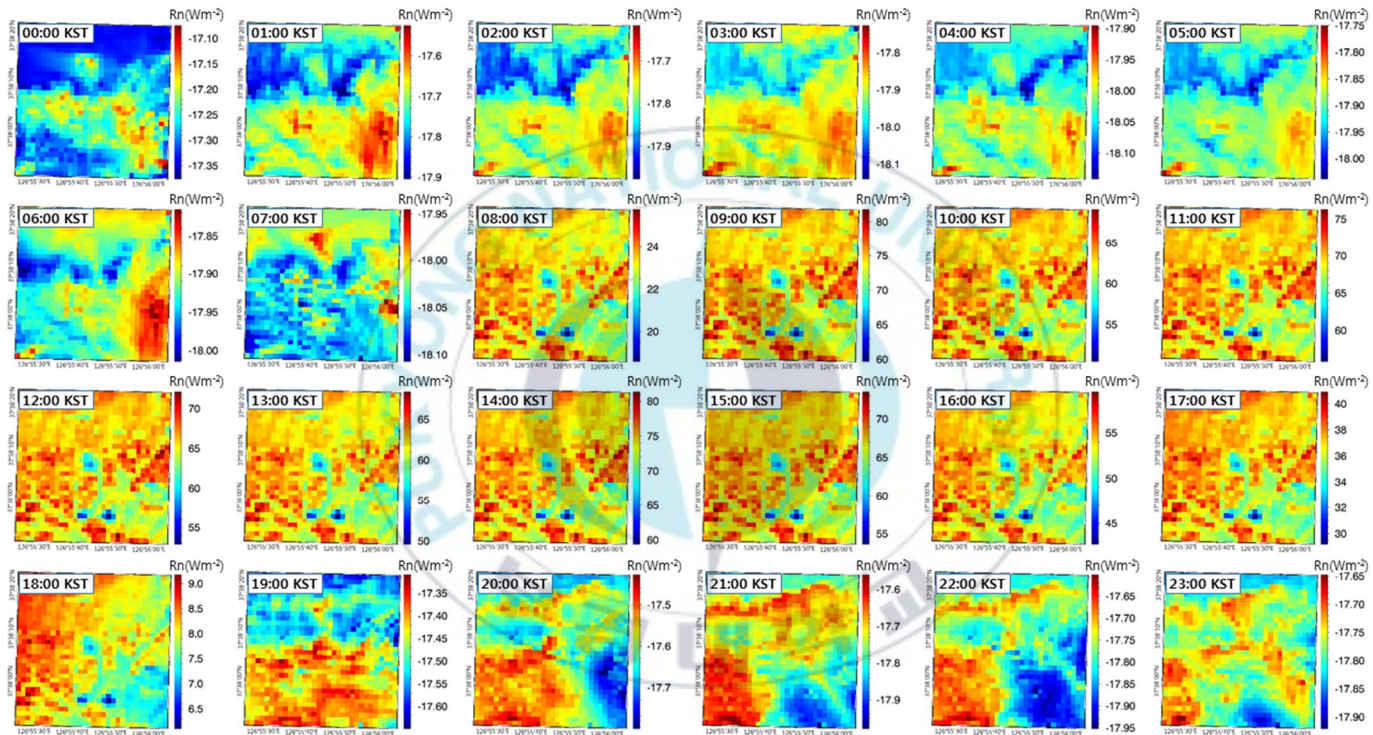


Figure 16. The spatial distribution of net radiation changes during the day, September 3<sup>rd</sup>, 2014, which is the area of this study.

#### 4.2.2. Validation with Eunpyeong Flux tower data

Based on the results of the spatial distribution shown in Section 4.2.1., we validation with the estimated Rn and measured Rn at the Eunpyeong flux tower.

Figure 17 is time serious graph showing observations and calculated Rn in time. The black line is the measured Rn data and red line is the estimated Rn data. This shows that the weekly trend is similar to flux tower as a whole. In Figure 17, also, it can be seen that the Rn of the darkened period has a relatively low value compared to the other days because it is the period during which cloudy or precipitation was present and the radiation has a tendency to change due to weather. The pattern in which Rn decreases during the summer period is due to precipitation conditions (Andre and Viswanadham, 1983; Heitor et al., 1991; Kim et al., 2013). We confirmed that the Rn calculated from these results are continuous, and reflect the effects of weather.

As a result of validation during the study period, the total RMSE of day and night is  $54.29 \text{ Wm}^{-2}$ , Bias  $27.42 \text{ Wm}^{-2}$  and  $R^2$  0.60. And the daytime RMSE is  $71.12 \text{ Wm}^{-2}$ , Bias  $25.66 \text{ Wm}^{-2}$  and  $R^2$  0.86 (Figure 18). This score is similar to the accuracy of Bisht and Bras (2011) and Ando and Ueyama (2017) (Table 4). Bisht and Bras(2011) used a Surface

Radiation Budget (SRB) to produce  $R_n$ , and Ando and Ueyama (2017) used a Eddy covariance method.

Figure 19 shows the time serious graph that the average of each time-of-the-study period and the result of validation. Overall, we confirm that the estimated data was overestimated than measured data. And the result of the analysis show the daytime RMSE  $33.65 \text{ Wm}^{-2}$ , Bias  $24.65 \text{ Wm}^{-2}$  and  $R^2$  0.96.



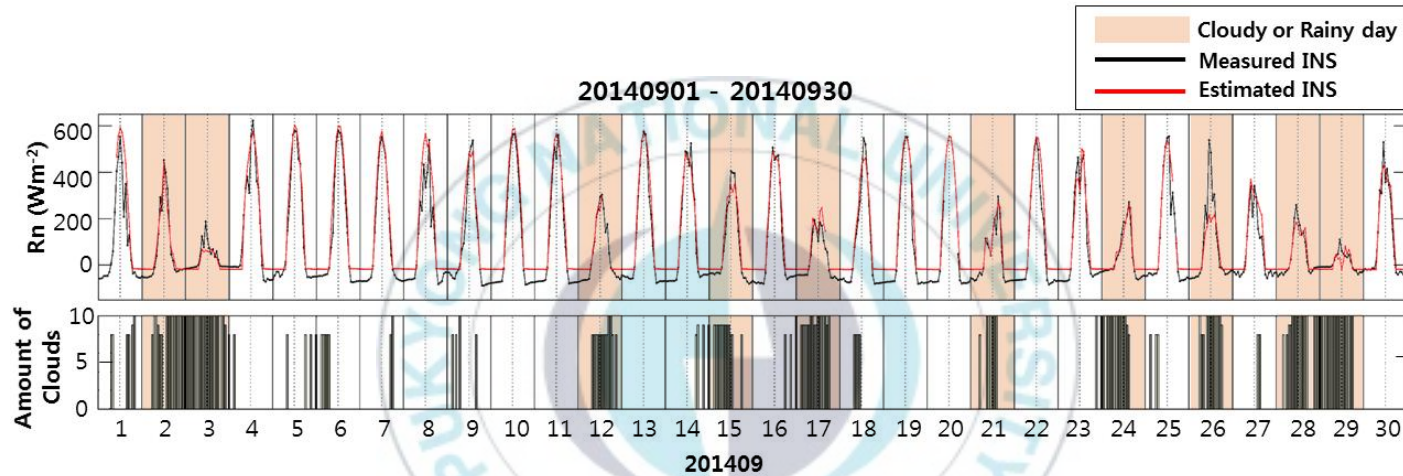


Figure 17. Time series for observed and estimated net radiation at Eunpyeong flux tower in Sep. 2014. The black dotted line is the observed and red triangle line is the estimated net radiation data. (upper) The graph is change of net radiation over time during the study period. (below) And the graph at the bottom is the amount of clouds during the study period. The parts of shadow are periods of cloudy or rainy days.

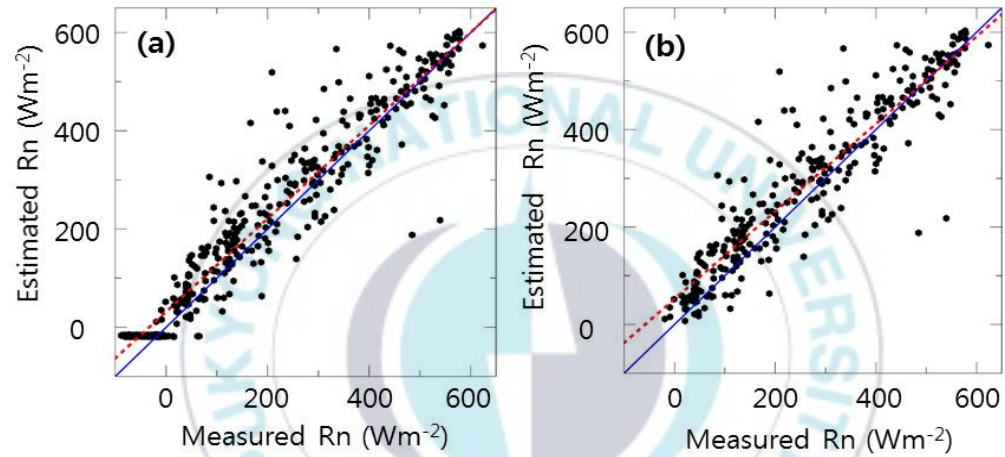


Figure 18. Result of correlation analysis between (a) the observed net radiation data at Eunpyeong flux tower and the estimated net radiation data during the day and (b) during the day time.

Table 4. The score of correlation analysis between net radiation at flux tower and hourly or hourly mean net radiation data at same pixel. And the result of previous studies (Bisht and Bras (2011) and Ando and Ueyama (2017)).

-	Region	RMSE ( $Wm^{-2}$ )	Bias ( $Wm^{-2}$ )	USE
<b>Fig.20 (b)</b>	Eunpyeong, Seoul	54.29	27.42	COMS & CFD model
<b>Bisht and Bras (2011)</b>	Penn State, US	72.01	-	Surface Radiation Budget (SRB)
<b>Ando and Ueyama (2017)</b>	Sakai, Japan	50.52	-	Eddy covariance

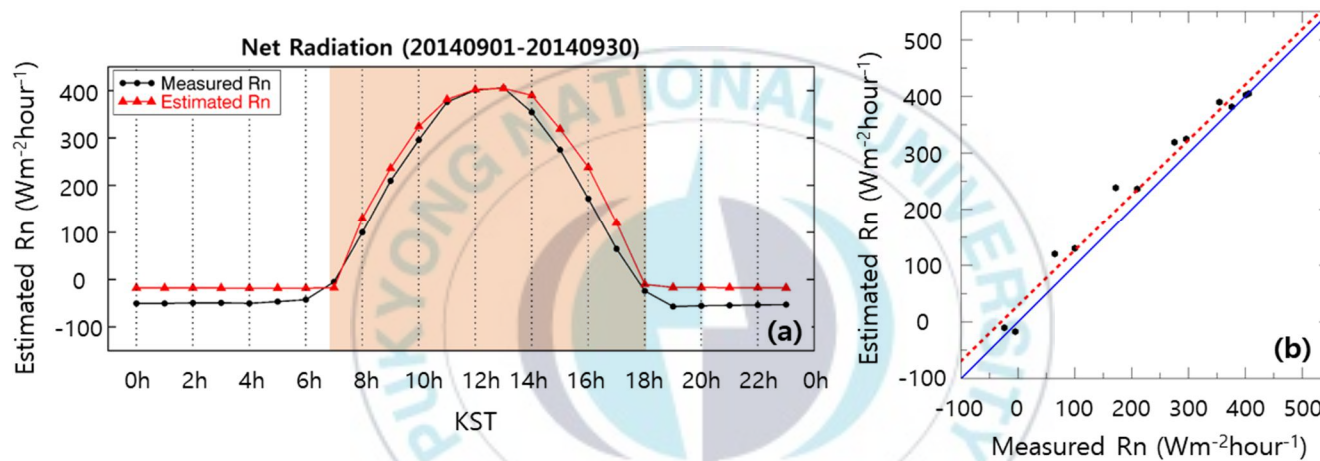


Figure 19. Result of the (a) time series during the study period (Sep. 2014.) and (b) correlation analysis between observed and estimated net radiation that the data calculated hour mean at Eunpyeong flux tower during the same period and daytime.

## 5. SUMMARY AND CONCLUSIONS

In this study, we retrieved and analyzed high resolution Rn using COMS satellite and CFD model data. This method of this study for Rn was first attempted at national and international. The calculated INS was corrected for the error, and the Rn from the urban area was calculated using the Ta simulated through the CFD model and the albedo data based on Landsat-8 satellite. This study calculated Rn including high temporal and spatial resolution compared with other previous studies.

We performed the validation of Rn between retrieved and measured at the Eunpyeong flux tower. Overall overestimated was measured Rn, but in the case of daytime, it has high accuracy of 54.29 Wm<sup>-2</sup>, Bias 27.42 Wm<sup>-2</sup> and R<sup>2</sup> 0.60. And the daytime RMSE is 71.12 Wm<sup>-2</sup>, Bias 25.66 Wm<sup>-2</sup> and R<sup>2</sup> 0.86. Also, when compared with the land cover map, it was confirmed that the Rn in the vegetation area and the urban area was retrieved similar to the land cover map. And that the Rn for periods of cloudy or precipitation have lower values and fluctuations than other clear days. This is a characteristic of radiation affected by weather conditions, and it is also related to Ta. However, in the case of Rn at night, unlike observed data where the variability is noticeable, we can see that the retrieved Rn is almost constant. This is because there is no INS at night,

and as a result, the short wave radiation part corresponding to one term is excluded in the  $R_n$  calculation. Therefore, it is considered that additional research is needed on the part related to the long wave radiation. If there is enough data to retrieve  $R_n$  and solve the long wave radiation, then the chance of further analysis related to urbanization and heat island phenomena will be possible. - The heat island phenomenon refers to the phenomenon that the temperature in the center of the city is significantly higher than the surrounding area due to the increase in population, various artificial facilities, concrete cover and automobile traffic, release of artificial heat, and greenhouse effect. - The reason for heat island, it appears more noticeably in the winter than in the summer, and more in the night than in the summer. Furthermore, since  $R_n$  can be an indicator of phenomena such as heat island phenomena and urbanization, it is important to understand the  $R_n$  distribution and changes in urban areas.

The results of this study can be used as a reference in the field related to agricultural, fisheries, and climate. It can also be used as an input data to the model of evapotranspiration which affects the global climate system and plays a crucial role in determining the characteristics of surface vegetation, thereby enhancing the accuracy of the model.

## 6. REFERENCES

- Alados, I., Foyo-Moreno, I., Olmo, F. J., & Alados-Arboledas, L. (2003). Relationship between net radiation and solar radiation for semi-arid shrub-land. *Agricultural and Forest Meteorology*, 116(3), 221-227.
- Anandakumar, K. (1999). A study on the partition of net radiation into heat fluxes on a dry asphalt surface. *Atmospheric Environment*, 33(24), 3911-3918.
- Ando, T., & Ueyama, M. (2017). Surface energy exchange in a dense urban built-up area based on two-year eddy covariance measurements in Sakai, Japan. *Urban Climate*, 19, 155-169.
- André, R. G. B., & Viswanadham, Y. (1983). Radiation balance of soybeans grown in Brazil. *Agricultural meteorology*, 30(3), 157-173.
- Asaeda, T., & Ca, V. T. (2000). Characteristics of permeable pavement during hot summer weather and impact on the thermal environment. *Building and Environment*, 35(4), 363-375.
- Bisht, G., and R.L. Bras, 2011. Estimation of net radiation from the Moderate Resolution Imaging Spectroradiometer over the continental United States. *IEEE Transactions on Geoscience and Remote Sensing*, 49(6), 2448-2462.
- Brutsaert, W. (1975). On a derivable formula for long-wave radiation from

- clear skies. *Water Resources Research*, 11(5), 742-744.
- Grimmond, S. (2007). Urbanization and global environmental change: local effects of urban warming. *The Geographical Journal*, 173(1), 83-88.
- Guoshui, L., Yu, L., & Di, X. (2011). Comparison of evapotranspiration temporal scaling methods based on lysimeter measurements. *Journal of Remote Sensing*, 15(2), 270-280.
- Hanna, S. R., Hansen, O. R., Ichard, M., & Strimaitis, D. (2009). CFD model simulation of dispersion from chlorine railcar releases in industrial and urban areas. *Atmospheric environment*, 43(2), 262-270.
- Harshan, S., Roth, M., Velasco, E., & Demuzere, M. (2017). Evaluation of an urban land surface scheme over a tropical suburban neighborhood. *Theoretical and Applied Climatology*, 1-20.
- Heitor, A., Biga, A. J., & Rosa, R. (1991). Thermal radiation components of the energy balance at the ground. *Agricultural and Forest Meteorology*, 54(1), 29-48.
- Hong, J. W. (2014). Effects of Residential Development on Sensible Heat Flux and Turbulence Characteristics. (Doctoral dissertation, Seoul National University Graduate School) (In Korean with English abstract).
- Hong, J. W., & Hong, J. (2016). Changes in the Seoul Metropolitan Area

- Urban Heat Environment with Residential Redevelopment. *Journal of Applied Meteorology and Climatology*, 55(5), 1091-1106.
- Hu, D., Cao, S., Chen, S., Deng, L., & Feng, N. (2017). Monitoring spatial patterns and changes of surface net radiation in urban and suburban areas using satellite remote-sensing data. *International Journal of Remote Sensing*, 38(4), 1043-1061.
- Idso, S. B., & Jackson, R. D. (1969). Thermal radiation from the atmosphere. *Journal of Geophysical Research*, 74(23), 5397-5403.
- IPCC, 2014: Climate Change 2014: Synthesis Report. Contribution of Working Groups I, II and III to the Fifth Assessment Report of the Intergovernmental Panel on Climate Change [Core Writing Team, R.K. Pachauri and L.A. Meyer (eds.)]. IPCC, Geneva, Switzerland, 151 pp.
- Jacobs, J., Mecikalski, J., & Paech, S. (2008). Satellite-based solar radiation, net radiation, and potential and reference evapotranspiration estimates over Florida. *Report prepared for the South Florida Water Management District*, 138.
- Kang, J.E., and J.J. Kim, 2017. Analysis of Wind Flow and Air Temperature in Urban Area Using CFD-UCM Model, Proc. Of the Autumn Meeting of KMS, Oct., pp. 583-584 (in Korean with English abstract).

- Kim, D., Baek, J., Jung, S. W., & Choi, M. (2013). Net Radiation Estimation Using Flux Tower Data and Integrated Hydrological Model: For the Seolmacheon and Chungmichen Watersheds. *Journal of Korea Water Resources Association*, 46(3), 301-314.
- Lee, D., Seo, M., Lee, K. S., Choi, S., Sung, N. H., Kim, H., ... & Han, K. S. (2016). Landsat 8-based High Resolution Surface Broadband Albedo Retrieval. *Korean Journal Of Remote Sensing*, 32(6), 741-746. (In Korean with English abstract).
- Lima, E. D. P., Sediyaama, G. C., Silva, B. B. D., Gleriani, J. M., & Soares, V. P. (2012). Seasonality of net radiation in two sub-basins of Paracatu by the use of MODIS sensor products. *Engenharia Agricola*, 32(6), 1184-1196.
- National Meteorological Satellite Center (2012). Insolation Algorithm Theoretical Basis Document, version 5, Korea Meteorological Administration, Korea.
- Nouri, H., Beecham, S., Anderson, S., Hassanli, A. M., & Kazemi, F. (2015). Remote sensing techniques for predicting evapotranspiration from mixed vegetated surfaces. *Urban Water Journal*, 12(5), 380-393.
- Ohring, G., & Clapp, P. (1980). The effect of changes in cloud amount on the net radiation at the top of the atmosphere. *Journal of the*

*Atmospheric Sciences*, 37(2), 447-454.

Pan, X., Liu, Y., & Fan, X. (2015). Comparative assessment of satellite-retrieved surface net radiation: An examination on CERES and SRB datasets in China. *Remote Sensing*, 7(4), 4899-4918.

Picón, A. J., Vásquez, R., González, J., Luvall, J., & Rickman, D. (2017). Use of remote sensing observations to study the urban climate on tropical coastal cities. *Revista Umbral (Etapa IV-Colección completa)*, (1), 218-232.

Roth, M. (2000). Review of atmospheric turbulence over cities. *Quarterly Journal of the Royal Meteorological Society*, 126(564), 941-990.

Trenberth, K. E., Fasullo, J. T., & Kiehl, J. (2009). Earth's global energy budget. *Bulletin of the American Meteorological Society*, 90(3), 311-323.

Wang, K., & Liang, S. (2008). An improved method for estimating global evapotranspiration based on satellite determination of surface net radiation, vegetation index, temperature, and soil moisture. *Journal of Hydrometeorology*, 9(4), 712-727.

Wright, J. L. (1982). New evapotranspiration crop coefficients. Proceedings of the American Society of Civil Engineers, *Journal of the Irrigation and Drainage Division*, 108(IR2), 57-74.

Xia, X. A., Wang, P. C., Chen, H. B., & Liang, F. (2006). Analysis of

downwelling surface solar radiation in China from National Centers for Environmental Prediction reanalysis, satellite estimates, and surface observations. *Journal of Geophysical Research: Atmospheres*, 111(D9).

Zhao, L., Lee, X., Smith, R. B., & Oleson, K. (2014). Strong contributions of local background climate to urban heat islands. *Nature*, 511(7508), 216.



## 7. APPELICES

### 7.1. Appendix 1: CMDPS Insolation Algorithm

The insolation (INS) can be calculated by using reflectance data and brightness temperature (TBB) data of stationary weather satellite. First, the most basic thing in calculating the INS is to obtain the atmospheric permeability. In general, the INS, which is incident on the top of the atmosphere, is calculated relatively simply by astronomical laws. However, it is not easy to estimate the amount of solar radiation in the ground because the solar energy that reaches the surface is scattered, reflected, and absorbed by elements such as air molecules, aerosols, ozone and clouds are present in the atmosphere. Therefore, it is important to parametrically quantify the effect of each element in the atmosphere in order to calculate the INS.

First, to calculate the INS reaching the surface, it is necessary to calculate the INS at the top of the atmosphere and calculate the amount of solar radiation that has been attenuated by the effects of scattering, reflection, absorption, etc. by the atmospheric elements. In this case, if there is a cloud, it can be calculated the INS by using the characteristics of clouds by satellite data and by applying the attenuation effects by the

cloud depending on the characteristic. But, it is extremely difficult to calculate the attenuation effects of clouds by using real satellite data because of the complicated physical characteristics of clouds. Therefore, in general, the error of the INS value calculated on the cloudy day is higher than the clear day.

The INS incident on the top of the atmosphere can be calculated as follows :

$$S = I \cdot (d_m / d)^2 \cdot \cos\theta \quad (7.1.1)$$

In the above equation, **I** mean the solar constant, and the value is 1367 Wm<sup>-2</sup>. And **(d<sub>m</sub> / d)<sup>2</sup>** is the elliptical eccentricity between the Earth and Sun. In the northern hemisphere, the elliptical eccentricity is the smallest in the winter and the largest in the summer. Also, since Korea is located in the middle latitude, the solar zenith angle is the lowest in summer and the highest value of solar radiation is observed. Where **d<sub>m</sub>** is the average distance and **d** is the actual distance between the Earth and Sun.

Finally, **S<sub>T</sub>**, total INS, can be calculated as follows using the atmospheric permeability for each atmospheric element calculated after the atmospheric parametrization process.

$$S_T = S_I + S_R + S_A \quad (7.1.2)$$

Where,  $S_I$  is direct INS,  $S_R$  is INS by Rayleigh scattering, and  $S_A$  is INS by aerosol scattering.

Clouds are the most difficult part of the atmospheric parametrization process. The reason for it is very difficult to parametrize the cloud with high temporal and spatial variability in a constant pattern. The calculation of cloud attenuation rate on the satellite uses the computed cloud reflectivity and temperature. The final surface INS value is calculated by multiplying the INS value of the clear sky and the attenuation by the cloud. The following equation can be used to calculate the INS at the surface when the cloud is present.

$$S = ( S_I + S_R + S_A ) \cdot ( 1 - a \cdot A ) \quad (7.1.3)$$

$$A = R / \cos\theta$$

Where  $A$  is the albedo and  $a$  is the INS attenuation factor by cloud. In the equation, the value is calculated by multiplying the total INS value at clear day by the cloud attenuation rate. In other words, in the case of a clear day without clouds, the  $S$  value is the INS value at surface because

the cloud albedo is 0, and when the cloud exists, the INS value is calculated by multiplying the INS of the cloudless clear day by the cloud attenuation rate.

In this INS calculation algorithm, the calculation of cloud damping coefficient using Cloud Factor (CF) is used differently than conventional methods (Kawamura et al., 1998; Tanahashi et al., 2001; Kawai et al., 2005).

The specific details of the change are as follows :

$$S_T = ( S_I + S_R + S_A ) \cdot CF \quad (7.1.4)$$

$$S_I = S \cdot (\tau_0 \cdot \tau_R - \alpha_w) \cdot \tau_A \quad (7.1.5)$$

$$S_R = S \cdot \tau_0 \cdot ( 0.5 \cdot ( 1 - \tau_R ) ) \cdot \tau_A \quad (7.1.6)$$

$$S_A = S \cdot (\tau_0 \cdot \tau_R - \alpha_w) \cdot F_C \cdot \omega_0 ( 1 - \tau_A ) \quad (7.1.7)$$

Here, the elements of each equation are the values absorbed, reflected and scattered by the atmosphere. Where  $\tau_0$  is transmitted by ozone absorption,  $\tau_R$  is transmitted by Rayleigh scattering,  $\alpha_w$  is the absorption rate of water vapor,  $\tau_A$  is transmitted by aerosol,  $F_C$  is the ratio of forward scattering to total scattering, and  $\omega_0$  is the single scattering albedo. The

total INS value calculated using each INS through atmospheric parametrization at the clear sky (Tanahashi et al., 2001).

